Multiple Morphological Profiles From Multicomponent-Base Images for Hyperspectral Image Classification

Xin Huang, *Senior Member, IEEE*, Xuehua Guan, Jón Atli Benediktsson, *Fellow, IEEE*, Liangpei Zhang, *Senior Member, IEEE*, Jun Li, *Member, IEEE*, Antonio Plaza, *Senior Member, IEEE*, and Mauro Dalla Mura, *Member, IEEE*

***Abstract*—Morphological profiles (MPs) are a useful tool for remotely sensed image classification. These profiles are constructed on a base image that can be a single band of a multicomponent remote sensing image. Principal component analysis (PCA) has been used to provide other base images to construct MPs in high-dimensional remote sensing scenes such as hyperspectral images [e.g., by deriving the first principal components (PCs) and building the MPs on the first few components]. In this paper, we discuss several strategies for producing the base images for MPs, and further categorize the considered methods into four classes: 1) linear, 2) nonlinear, 3) manifold learning-based, and 4) multilinear transformation-based. It is found that the multilinear PCA (MPCA) is a powerful approach for base image extraction. That is because it is a tensor-based feature representation approach, which is able to simultaneously exploit the spectral–spatial correlation between neighboring pixels. We also show that independent component analysis (ICA) is more effective for constructing base images than PCA. Another important contribution of this paper is a new concept of multiple MPs (MMPs), aimed at synthesizing the spectral–spatial information extracted from the multicomponent base images, and further enhancing the classification accuracy of MPs. Moreover, we propose two different strategies to interpret the newly proposed MMPs by considering their hyperdimensional feature space: 1) decision fusion and 2) sparse classifier based on multinomial logistic regression (MLR). Experiments conducted on three well-known hyperspectral datasets are used to quantitatively assess the accuracy of different algorithms.**

***Index Terms*—Feature extraction (FE), hyperspectral imaging, morphological profiles (MPs), spectral–spatial classification.**

Manuscript received March 30, 2014; revised June 17, 2014; accepted July 13, 2014. Date of publication August 26, 2014; date of current version January 21, 2015. This work was supported in part by the National Natural Science Foundation of China under Grant 41101336 and Grant 91338111, in part by the Program for New Century Excellent Talents, University of China under Grant NCET-11-0396, and in part by the Foundation for the Author of National Excellent Doctoral Dissertation of PR China (FANEDD) under Grant 201348.

X. Huang, X. Guan, and L. Zhang are with the State Key Laboratory of Information Engineering in Surveying, Mapping, and Remote Sensing, Wuhan University, Wuhan 430079, China (e-mail: huang_whu@163.com).

J. A. Benediktsson is with the Faculty of Electrical and Computer Engineering, University of Iceland, Reykjavik 107, Iceland.

J. Li is with the Guangdong Key Laboratory for Urbanization and Geo-Simulation, School of Geography and Planning, Sun Yat-sen University, Guangzhou 510275, China.

A. Plaza is with the Hyperspectral Computing Laboratory, Department of Technology of Computers and Communications, Escuela Politécnica, University of Extremadura, 10071 Cáceres, Spain.

M. Dalla Mura is with the Department of Image and Signal Processing (DIS), Grenoble Images Speech Signals and Automatics Laboratory (GIPSA-Lab), Grenoble Institute of Technology, Saint Martin d'Heres Cedex 38402, France.

Color versions of one or more of the figures in this paper are available online at http://ieeexplore.ieee.org.

Digital Object Identifier 10.1109/JSTARS.2014.2342281

I. Introduction

THE ADVENT of hyperspectral imagery, recording hundreds of spectral channels, has opened up new avenues for image analysis and information extraction, which provides additional capacities for remote sensing applications in many different areas, such as precision agriculture, urban mapping, environment management, military applications. Recently, hyperspectral data with high-spatial resolution have become available, which provides very wealthy information in both the spectral and spatial domains at the same time [1]. Consequently, for an accurate interpretation of this kind of imagery, it is indispensable to simultaneously exploit the radiometric information in the spectral domain and the structural information in the spatial domain. In this regard, joint spectral–spatial classification has received much interest, and a number of research papers have been published on this topic. Among these, several representative methods rely upon the use of MPs, which were originally proposed in [2] for high-spatial-resolution image classification, and subsequently, generalized as extended morphological profiles (EMPs) for hyperspectral data by constructing the MPs on the first PCs [3] (refer to Table I for all the acronyms that are used throughout the paper). MPs extract multiscale structural features by locally processing an image via a series of structural elements (SEs) with different sizes and hence exploit spatial information for improving the traditional pixelwise image spectral classification [4], [5]. Considering that the EMPs do not adequately take advantage of the spectral information for hyperspectral image classification, Fauvel *et al*. [6] proposed to further inject the spectral features extracted from the original hyperspectral bands into the MPs, forming a spectral–spatial hybrid feature space. A new development of the MPs is given by attributes profiles (APs), proposed by Dalla Mura *et al*. [7]. Unlike the traditional MPs performed on SEs with different sizes, APs aim to generate morphological profiles (MPs) by filtering the connected components of an image with different criteria. Similarly, APs were generalized to EAPs when applied to

TABLE I
LIST OF ACRONYMS

MMPs	Multiple morphological profiles
MPs	Morphological profiles
EMPs	Extended morphological profiles
PCA	Principal component analysis
ICA	Independent component analysis
MLR	Multinomial logistic regression
PCs	Principal components
ICs	Independent components
SEs	Structural elements
APs	Attributes profiles
EAPs	Extended attributes profiles
KPCA	Kernel PCA
NMF	Nonnegative matrix factorization
CNMF	Constrained nonnegative matrix factorization
FA	Factor analysis
KNMF	Kernel nonnegative matrix factorization
LPP	Locality-preserving projections
NPE	Neighborhood-preserving embeding
MPCA	Multilinear PCA
JADE	Joint approximation diagonalization of eigenmatrices
LORSAL	Logistic regression via variable splitting and augmented lagrangian
SVM	Support vector machine
ROSIS	Reflective optics systems imaging spectrometer
HYDICE	Hyperspectral digital imagery collection experiment

TABLE II
REVIEW OF THE CURRENT BASE IMAGES USED FOR MORPHOLOGICAL PROFILES

Profiles	Base images	References
EMPs	PCA	[3], [6], [10], [11]
	ICA	[13]
	KPCA	[12]
EAPs	PCA	[8]
	JADE-ICA	[15]
	KPCA	[16]

hyperspectral images by computing the APs based on the first PCs [8]. Other variants concerning MPs and APs involve directional morphological profiles [9] or multifeature fusion [10].

Both EMPs and EAPs exhibit good performance when used for spectral–spatial classification of hyperspectral imagery [53]. It should be noticed that a key issue for the extension of the morphological profiles is to determine a set of base images, on which the EMPs or EAPs are built. We define the base images as *one or several feature images, extracted from the original hyperspectral data, for the subsequent spatial/structural feature extraction and spectral–spatial classification*. Most of the base images considered in the existing literature are the first or first few PCs. However, additional strategies used for EMPs and EAPs can be summarized as follows (see Table II).

1) In the case of EMPs, the classification results of the EMPs built on the KPCA outperformed those obtained with the EMPs with the PCA, because the KPCA extracts more useful features for classification [12]. The limitation of the KPCA, however, is its computational cost, caused by the kernel-based feature representation [12]. In addition, more base images are needed for KPCA to achieve a satisfactory result, which always leads to a more significant computational burden. With respect to ICA, it has been shown that it led to equivalent results to the PCA in terms of classification accuracy [13], [14].
2) In the case of EAPs, it has been proved that ICA is more suitable than PCA for constructing thebase images for the EAPs [15].

TABLE III
BASE IMAGES CONSTRUCTION METHODS CONSIDERED IN THIS STUDY FOR GENERATING THE MORPHOLOGICAL PROFILES

Category	Method
Linear	PCA, JADE-ICA, Fast-ICA, CNMF, FA
Nonlinear	KPCA, KNMF
Manifold	LPP, NPE
Multilinear	MPCA

The methods used to construct base images for the first time in the literature are underlined.

In this paper, we focus on unsupervised methods, which are data-driven, self-adaptive, and automatic, for generating base images of MPs. A detailed comparison between unsupervised and supervised methods is conducted in Section V-E.

Based on the aforementioned analysis, we conclude that, although a few studies exist, most of the base image construction methods are related to traditional feature extraction (FE) techniques. A systematic investigation and a general conclusion are lacking, especially, for EAPs. As a result, an important objective of this work is to conduct a systematic study on the base images used for the morphological profiles (both EMPs and EAPs), and extend the current framework by proposing a series of new methods, e.g., multilinear transformation [17], and manifold learning [18]-based. As shown in Table III, the base images considered in this study include the following four categories.

1) *Linear transformations*: In this category, base images are extracted from the hyperspectral imagery via linear transformations. To our knowledge, the Fast-ICA [19], CNMF [20], and the FA [21] are used to construct base images of MPs for the first time in this work.
2) *Nonlinear transformation*: Since hyperspectral data exhibit intrinsic nonlinear properties [22], nonlinear transformations can also be appropriate for the construction of base images. In this paper, two representative kernel-based transformations, KPCA [12] and KNMF [23], are employed.
3) *Manifold learning*: This strategy aims to seek a manifold coordinate system that preserves geodesic distances in high-dimensional data space [24]. The manifold coordinate representation is able to exploit the nonlinear structure of hyperspectral imagery and hence discriminate between spectrally similar classes [24]. Therefore, manifold learning is also a suitable strategy for producing base images for MPs. Based on this observation, we propose to adopt two manifold transformation algorithms for base image extraction in this work, LPP [25] and NPE [26].

4) *Multilinear transformation*: Hyperspectral data can be naturally represented as a 3-order tensor with the joint spatial–spectral dimensions. However, traditional FE methods process the whole image in a vector-based manner, which does not exploit the spatial correlation between neighboring pixels and hence ignore the discriminative information in the image local structure. In this context, we propose in this work to use multilinear transformation (e.g., multilinear PCA [27]) for creating the base images of hyperspectral imagery.

It should be noted that traditional EMPs or EAPs are built on a single kind of base images. However, the morphological features derived from various base images can complement each other and contribute to the final classification based on the multiple profiles. Consequently, another contribution of this work is the introduction of MMPs, which integrate the MPs (EMPs or EAPs) extracted from multiple base images. Specifically, two new strategies are introduced in this work for taking advantage of MMPs for hyperspectral image classification.

1) *Stacked MMPs*: A natural way to integrate the discriminative information from the MMPs is to classify the stacked profiles derived from multiple base images. However, this strategy poses a great challenge to the classifier, since the concatenation of MMPs necessarily leads to a hyperdimensional feature space and a huge computational burden needs to be employed for the classification process. In this work, we propose to use SVMs [28] for interpreting the MMPs, along with LORSAL algorithm [29], which is a recently developed classifier with low computational complexity.
2) *Decision fusion of MMPs*: Another strategy for information mining from the MMPs is decision fusion, where a series of subclassifiers are used for each category of profiles.Then, the information from the outputs of the subclassifiers is further integrated for the final decision. The decision fusion is able to reduce the computational burden for the classification of MMPs [10].

In order to provide an experimental validation of the newly introduced approaches, we have conducted an evaluation of three well-known public hyperspectral datasets with high-spatial resolution: ROSIS, Pavia University and Centre, and HYDICE DC Mall. The remainder of this paper is organized as follows. Section II briefly introduces the morphological profiles (EMPs and EAPs), followed by the FE algorithms used for the extraction of base images in Section III. The new techniques developed for information fusion and classification based on the proposed MMPs are described in Section IV. Experimental results and analysis are presented in Section V, and Section VI concludes this study with some remarks and hints at plausible future research.

II. Morphological Profiles

A. Extended MPs

Mathematical morphology is based on two fundamental operators: erosion and dilation [30]. Morphological opening aims to dilate an eroded image to filter out bright structures, while morphological closing aims to erode a dilated image to suppress dark structures. It is generally desirable that a reconstruction filter is implemented on these basic morphological operators in order to preserve original image structures and suppress shape noise [31]. The opening and closing operators have been proven to be both effective in analyzing spatial interpixel dependence and dealing with the spatial information for classification of high-spatial-resolution images [9], [32].

Let $\gamma^{SE}(I)$ and $\phi^{SE}(I)$ be the morphological opening and closing with a SE [30] for an image I. MPs are defined by a series of SEs with increasing sizes

$$\begin{aligned} \mathrm{MP}_\gamma &= \{\mathrm{MP}_\gamma^\lambda(I) = \gamma^\lambda(I), \quad \forall\lambda \in [0,n]\} \\ \mathrm{MP}_\phi &= \{\mathrm{MP}_\phi^\lambda(I) = \phi^\lambda(I), \quad \forall\lambda \in [0,n]\} \\ &\text{with} \quad \gamma^0(I) = \phi^0(I) = I \end{aligned} \tag{1}$$

where λ represents the radius of a disk-shaped SE which is commonly used in the literature [3], [11], [33]. MPs based on opening/closing by reconstruction are generated from a gray level image using a set of SEs with gradually increasing sizes, representing the multiscale information of the image. However, as previously stated, when dealing with hyperspectral images, it is impractical to directly calculate the MPs for each spectral band, since it would lead to a hyperdimensional feature space showing a large amount of information redundancy.

In this context, EMPs [3] have been proposed for morphological FE from hyperspectral imagery. EMPs contain a series of MPs built on the so-called base images, which contain a few bands but represent most of the information which is relevant for discrimination purposes in the original hyperspectral image. EMPs can be written as

$$\mathrm{EMP} = \{\mathrm{MP}(f(1)), \mathrm{MP}(f(2)), \ldots, \mathrm{MP}(f(n))\} \tag{2}$$

where f comprises a set of the n-dimensional base images.

B. Extended Morphological Attribute Profiles

Morphological attribute filters represent an adaptive morphological analysis technique which implements a series of attribute thickening and thinning operators on connected components, according to various criteria [34]. For each connected component, if the criterion is verified then the connected component is kept unaffected. Otherwise, the connected component might be removed (the removal is subject to the filtering rule employed when nonincreasing attributes are considered). APs can be expressed within the framework of MPs defined in (1), by replacing the opening and closing operators by a series of morphological attributes. Let us denote by $\gamma^{T_\lambda}(I)$ and $\phi^{T_\lambda}(I)$, the attribute thinning and thickening operators, respectively. With a criterion T_λ, the APs can be written as

$$\begin{aligned} \mathrm{AP}_\gamma &= \{\mathrm{AP}_\gamma^{T_\lambda}(I) = \gamma^{T_\lambda}(I) \quad \forall\lambda \in [0,n]\} \\ \mathrm{AP}_\phi &= \{\mathrm{AP}_\phi^{T_\lambda}(I) = \phi^{T_\lambda}(I) \quad \forall\lambda \in [0,n]\} \\ &\text{with} \;\; \gamma^{T_0}(I) = \phi^{T_0}(I) = I. \end{aligned} \tag{3}$$

The morphological attributes considered in this paper involve the area of the regions, the length of the diagonal of the bounding box, the first moment of inertia, and the standard deviation [7]. In this way, based on the various attributes and the multilevel criteria considered, an image can be represented by a set of multilevel spatial and spectral features. As it was

already the case with EMPs, when processing hyperspectral imagery, the EAPs are generated from a series of base images as follows:

$$\mathrm{EAP} = \{\mathrm{AP}(f(1)), \mathrm{AP}(f(2)), \ldots, \mathrm{AP}(f(n))\}. \quad (4)$$

III. Extraction of Base Images

In this section, we analyze several FE methods used to generate the base images from the hyperspectral data. The considered methods are split into four categories, i.e., linear transformations, nonlinear transformations, manifold learning, and multilinear transformations.

A. Linear Transformations

The linear model can be defined as a linear subspace of the original hyperspectral bands

$$Y = \Phi^T X \quad (5)$$

where X is the input data, Y is the output data, and Φ is a transformation matrix [33]. The transformation matrix Φ is calculated by optimizing a specific objective function. In this study, several representative linear models are considered, including PCA, ICA, NMF, and FA. In the following, we briefly outline these methods.

1) Principal Component Analysis: Principal component analysis (PCA) generates base images by analyzing the covariance matrix of the original hyperspectral images. The PCA transformation for a hyperspectral image is achieved by

$$Y_{\mathrm{PCA}} = V^T(X - m) \quad (6)$$

where the transformed component Y_{PCA} is obtained by projecting the original feature space into a subspace which contains a majority of the cumulative covariance by analyzing the mean (m) and the eigenvector (V) of the hyperspectral data. PCA has been shown not to be optimal for the classification [35]. However, from the FE point of view, PCA is able to represent the original hyperspectral data using only a few principal components. Therefore, it is still the most widely used method for generating the base images for MPs.

2) Independent Component Analysis: Independent component analysis (ICA) has been adopted as a method for constructing base images for EMPs and EAPs for hyperspectral FE [13], [15]. It is a multivariate data analysis method for blind source separation of signals which seeks to render the components as statistically independent as possible. The basic model of ICA is

$$Y = W_{\mathrm{ICA}}^T X \quad (7)$$

which aims to find a separating matrix W and generate a few independent components (ICs) by solving the statistical independence function. Two representative ICA algorithms are carried out in this study:

a) Fast-ICA [19]: It is a fixed-point algorithm based on an optimization of negative entropy function. Specifically, Fast-ICA is realized by maximizing

$$J_G(w) = \left[E\{G(w^T x)\} - E\{G(v)\}\right] \quad (8)$$

subject to $E\{(w^T x)^2\} = 1$, where the function $G(\cdot)$ is a sufficiently regular nonquadratic function, and v is a standardized Gaussian variable. $E\{G(w^T x)\}$ is the Gaussian moment of the data. The fast-ICA algorithm estimates the independent components one by one using a deflation scheme [19].

b) Joint approximation diagonalization of eigenmatrices-ICA [36]: The JADE algorithm aims at exploiting the higher order statistics and performing joint diagonalization on the cumulant matrix. The optimization process can be described by the following function [36]:

$$\hat{V} = \arg\min \left(\sum_i \mathit{Off}\,(V^* Q_i^Z V) \right) \quad (9)$$

where V is an orthonormal transformation matrix of the whitened data, Q_i^Z is a maximal set of cumulant matrices, $\hat{V}$ is the rotation matrix, and V^* is the generalized inverse of V. The function *Off* denotes the sum of the squares of the nondiagonal elements of a matrix.

3) Nonnegative Matrix Factorization: The NMF method, originally proposed for human face recognition [37], is an effective approach for multivariate data analysis. It has been successfully applied to endmember analysis and FE for hyperspectral imagery [38], [39]. NMF aims to transform high-dimensional data into a low-dimensional and nonnegative linear subspace. Given a high-dimensional observed feature $x \in R_{L\times N}^+$ and a basic coefficient vectors $A = [a_1, a_2, \ldots, a_p]$, a linear approximation of the data can be described by

$$x_i \approx AS_i, \quad i = 1, \ldots, N \quad \text{s.t.} \quad S_i \geq 0, \quad A \geq 0 \quad (10)$$

where $S \in R_{L\times N}^+$ is the weight coefficient matrix. To solve the nonnegative condition of NMF, different constraints can be imposed on the objective function. One natural way is to realize

$$\min f(A, S) = \|X - AS\|. \quad (11)$$

In this study, a constrained NMF, which was recently developed for hyperspectral unmixing in our previous work [20], is adopted here to generate the base images from hyperspectral images. The CNMF algorithm improves the original NMF by considering an additional spectral dissimilarity measure, which is defined by the spectral gradient. One can refer to [20] for additional details.

4) Factor Analysis: Factor analysis (FA) is able to search for the possible underlying factor structure of a set of measured variables without imposing any preconceived structures on the outputs [21]. A factor is defined as an unobservable feature that is assumed to influence the observed ones. The goal of FA is to reveal such relations, and thus can be used to reduce the feature dimension [40]. Specifically, an N-dimensional variable X is reduced to a K-dimensional variable Z by the following transformation:

$$Z = E(Z|X) = (I + \Lambda^T \Psi^{-1} \Lambda)^{-1} \Lambda^T \Psi^{-1}(X - \mu) \quad (12)$$

where Λ and Ψ are randomly initialized, and Ψ is not singular. μ is the mean of the N-dimensional vectors. More details about FA can be found in [40].

The linear transformations, such as PCA or ICA, are currently the most widely used methods for generating base

images. In this study, the NMF and FA algorithms are considered for extracting base images for MPs for the first time. NMF is a nonnegative part-based image representation approach, which is appropriate for the subsequent morphological FE. FA has a potential for identification of groups of interrelated variables and reduction of number of variables, by combining two or more variables into a single factor [41]. Therefore, FA is consistent with the definition of base images and it is interesting to see its performance for generating MPs.

B. Nonlinear Transformations

Compared to the linear transformations, nonlinear methods are capable of capturing higher order statistics and, hence, exhibit potential to better represent the hyperspectral information. Accordingly, the KPCA has been used to generate base images for EMPs [12], [33] and EAPs [16]. In this study, in addition to the KPCA, the KNMF is also tested in regards to its capacity to provide base features.

The basic principle of kernel mapping is to project the original feature space, in which the classes of interest cannot be linearly separated, into a higher dimensional space, in which these classes may be linearly separated. The kernel method realizes this nonlinear mapping via the function

$$K(x, y) = \Phi(x) \cdot \Phi(y) \tag{13}$$

which is defined by specifying the inner product in the feature space. The KPCA and KNMF algorithms are briefly introduced below.

1) Kernel PCA: KPCA aims at solving the following eigenvalue problem:

$$\lambda v = Kv, \quad \text{s.t.} \quad \|v\|_2 = \frac{1}{\lambda} \tag{14}$$

where K is the kernel of KPCA that can convert the dot product in the feature space to a function in the input space. Similar to PCA, the first k principal components derived from KPCA can be extracted according to the eigenvector ranking. Readers can refer to [12] for details.

2) Kernel NMF: As mentioned above, NMF is an efficient method for hyperspectral image representation. NMF has been extended to a kernel version, KNMF, which is able to extract nonlinear features hidden in the original data [23]. KNMF can be derived from the framework of NMF. Given a higher or infinite dimensional feature space, the nonlinear mapping can be expressed by

$$x_i \to \phi(x_i) \text{ or } \mathrm{X} \to \phi(\mathrm{X}) = (\phi(x_1), \ldots, \phi(x_n)). \tag{15}$$

Similar to NMF, the KNMF decomposition can be represented by $\phi(X) \approx A_\phi S$. In the convex NMF model [56], A_ϕ is restricted to a convex combination of the observed features $A_\phi = x_i G$ with negative coefficient G. Therefore, KNMF is realized by the following objective function:

$$\begin{aligned} \|\phi(X) - A_\phi(S)\|^2 &= \|\phi(X) - \phi(X)GS\|^2 \\ &= \mathrm{Tr}\left[\phi(X)^T\phi(X) - 2\mathrm{S}\phi(X)^T\phi(X)\mathrm{G} \right. \\ &\quad \left. + G^T\phi\,(X)^T\phi(X)\mathrm{GS}S^T\right]. \end{aligned} \tag{16}$$

From (16), it can be seen that the transformation depends only on the kernel.

C. Manifold Learning

Manifold learning seeks for an embedded nonlinear manifold within the higher dimensional space (e.g., hyperspectral data). It is able to reduce the dimensionality of the original data and represent its intrinsic structure by constructing nonlinear low-dimensional manifolds. Manifold learning has been introduced for representation of the hyperspectral information by deriving a manifold coordinate system from the geodesic distances between pixels of the underlying nonlinear hyperspectral data manifold [24]. It should be noted that, to our knowledge, manifold learning has not been used previously for producing base images for MPs. Accordingly, in this paper, two manifold algorithms, LPP and NPE, are considered.

1) Locality-Preserving Projections: LPP represents image data by building a graph which can model the neighborhood information [25]. It is able to preserve the local structure of the image space by explicitly considering the manifold structure. It is solved by optimizing a generalized eigenvalue problem

$$XLX^TA = \lambda XDX^TA \tag{17}$$

where $D_{ii} = \sum_j W_{ij}$ is a diagonal matrix and $L = D - W$ is the Laplacian matrix. The mapping achieved by transformation A can be realized by minimizing the objective function

$$\min \sum_{i,j=1}^{n} \|y_i - y_j\|^2 W(i, j) \tag{18}$$

where $y_i = A^T x_i$ and the weight matrix W is constructed via the nearest-neighbor graph.

2) Neighborhood-Preserving Embedding: NPE is a linear approximation ofthe locally linear embedding (LLE) [42], which makes it fast and suitable for practical implementation. Given a set of points $x_1, x_2, \ldots, x_m$ in the ambient space, an adjacency graph is firstly constructed to describe the relationship between neighboring pixels. The weights of the edges for the graph are computed by minimizing the objective function

$$\min \left\| x_i - \sum_{j \in N_k(x_j)} W_{ij} x_j \right\|^2, \quad \text{s.t.} \sum_{j \in N_k(x_j)} W_{ij} = 1. \tag{19}$$

Subsequently, the linear projection is obtained by solving the following generalized eigenvector problem:

$$\mathrm{XM}X^Ta = \lambda XX^Ta \tag{20}$$

where $M = (I - W)^T(I - W)$. For more details about NPE, readers can refer to [26].

D. Multilinear Transformation

Multilinear PCA [27], which extends the original PCA by representing the data as tensors, has been recently explored for hyperspectral image classification [43]. The conventional PCA vectorizes the tensor data, leading to insufficient representation for remote sensing imagery. The MPCA that aims to extract the hyperspectral image as a cube (third-order tensor) is, however, more suitable for representing the spectral–spatial information of the original data. In analogy to the PCA, MPCA is carried out by the following steps.

1) *Centralization*: A tensor sample χ is subtracted by its mean $\bar{\chi}^{(N)}$, resulting in a centered tensor χ^c, which can be decomposed using high-order SVD (HOSVD) [17] as follows:

$$\chi^c = S \times_1 U^{(1)} \times_2 U^{(2)} \times \cdots \times_N U^{(N)} \tag{21}$$

where S is the core tensor, $U^{(N)}$ is the basic matrix, and $S \times_N U^{(N)}$ is the N-mode product of a tensor S by a matrix U.

2) *Orthonormal projection*: The HOSVD of χ^c is truncated by keeping the first R_n columns for the basismatrix $U^{(n)}$ in each mode to produce $\tilde{U}^{(n)}$, which is associated with the most significant eigentensors. The tensor projection can thus be achieved by

$$\bar{P}_{-N} = \times_1 \tilde{U}^{(1)^T} \times_2 \tilde{U}^{(2)^T} \times \cdots \times_N \tilde{U}^{(N)^T}. \tag{22}$$

3) *Dimensionality reduction*: A centered input tensor Z^c of order $(N-1)$ is projected to a tensor subspace by

$$\begin{aligned} \bar{y} &= Z^c \times \bar{P}_{-N} \\ &= Z^c \times_1 \bar{U}^{(1)^T} \times_2 \bar{U}^{(2)^T} \times \cdots \times_N \bar{U}^{(N)^T}. \end{aligned} \tag{23}$$

For more details about MPCA, readers can refer to [17] and [27].

IV. Multiple Morphological Profiles

An important objective of this study is to investigate and assess the performance of different FE methods for the generation of base images from hyperspectral imagery. It should be noted that one can obtain a set of MPs from multiple base images. Considering the different principles and the possible complementarities among these base images, it is worth attempting to construct multiple MPs, which have the potential to better represent the spectral–spatial characteristics of the hyperspectral imagery.

Naturally, there are two strategies for exploiting the MMPs for hyperspectral image classification (see Fig. 1). The first one is to classify the stacked MMPs. In this case, it should be noted that a linear classifier is adequate since the construction of MMPs leads to hyperdimensional data and a sparse feature space, which has sufficient discriminative information for classification. Nonlinear classifier, such as the kernel-based SVM, which projects the original feature space into a higher dimensional space in order to enhance the separability, may complicate the problem and lead to overfitting of the classification model for the MMPs. In this study, an efficient solution to this problem is discussed in Section IV-A. The other strategy is to carry out a decision fusion on the MMPs, i.e., the MMPs are individually interpreted using a set of subclassifiers and the decision results are then synthesized via a fusion rule. In this way, one can avoid the related issues resulting from the classification of the hyperdimensional feature. The aforementioned two strategies are explained in detail as follows. It should be underlined that the contribution of this paper refers to the concept of MMPs, but not to the feature fusion algorithms.The stacking or decision fusion is one of the specific methods for carrying out the MMPs for classification.

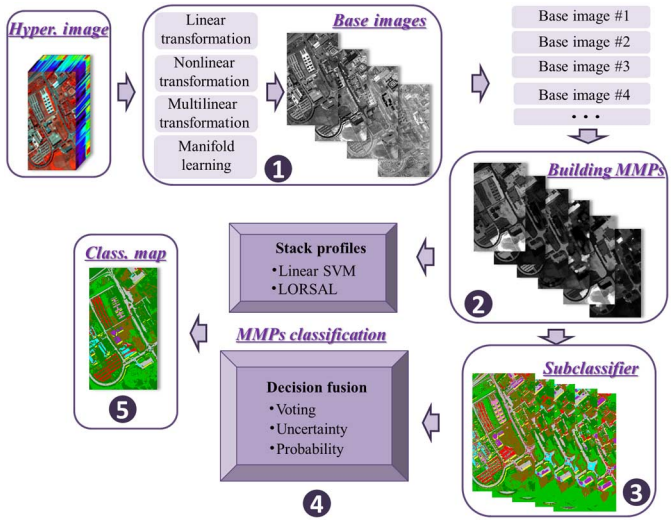

Fig. 1. General framework of this study.

A. Stacked MMPs

In this work, we propose to use the multinomial logistic regression (MLR) [44] to classify the stacked MMPs taking into account its capability for processing hyperdimensional data. MLR [44] as well as its sparse version SMLR (sparse MLR) [45]–[47], modeling the class posterior densities instead of the joint probability distribution, has the advantage of being able to adequately interpret very high-dimensional feature spaces. The fast SMLR algorithm [48], which optimizes the applicability of SMLR to high-dimensional datasets, has proved to be efficient for classification of hyperspectral images [49], [50]. More recently, the LORSAL algorithm [29] has been proposed to further significantly reduce the complexity to learn the MLR classifier. The basic principle of the LORSAL algorithm is to replace a difficult nonsmooth convex problem with a set of quadratic and diagonal problems, which are much easier to solve [50]. Therefore, LORSAL is used here to interpret the hyperdimensional stacked MMPs. For more details about LORSAL, readers can refer to [50] and [52].

B. Decision Fusion

Decision fusion is also an efficient approach for processing MMPs. Specifically, the morphological profiles derived from different base images are classified separately and the final decision result is obtained by a fusion rule. In this study, the following three rules are used.

1) Voting: Majority voting selects the label that receives the largest votes from a series of subclassifiers as the final result [51]

$$C(x_r) = \arg\max_k \left(\mathrm{Vote}_k(x)\right) \tag{24}$$

where $C(x_r)$ is the decision result for pixel x and $\mathrm{Vote}_k(x)$ is the number of votes for class k ($k = 1, \ldots, K$).

2) Probability: The second decision fusion strategy is based on the posterior probabilities, which actually compares the soft output of the L subclassifiers [10]

$$C(x_r) = \arg\max_k \sum_{l=1}^{L} p_l^k(x) \tag{25}$$

where $p_l^k(x)$ is the posterior probability of pixel x belonging to class k with the lth classifier.

3) Uncertainty: The certainty of the classification for each pixel can be assessed based on its posterior probabilities [10]. A large value of certainty signifies the classification for the pixel is reliable. Consequently, the certainty measure can be used as the weight of the probabilistic output in order to enhance the reliability of the voting. By considering the classification certainty measure $S(x)$ for each pixel, (25) can be extended to

$$C(x_r) = \arg\max_k \left\{ \frac{1}{L} \sum_{l=1}^{L} S_l(x) \cdot p_l^k(x) \right\}$$
$$\text{with } S(x) = \sum_{k=1}^{K-1} [\hat{p}_k(x) - \hat{p}_{k+1}(x)] \cdot \frac{1}{k} \tag{26}$$

where $\hat{p}_1(x), \ldots, \hat{p}_k(x), \ldots, \hat{p}_K(x)$ represents the class probabilistic outputs in a descending order.

V. Experiments

A. Datasets and Experimental Setting

The experiments are carried out using three hyperspectral images. The first two datasets widely used hyperspectral images for model validation, which were acquired over the city of Pavia (Italy) by the ROSIS-03 sensor. For these datasets, both images have a spatial resolution of 1.3 m with 115 spectral bands, ranging from 0.43 to $0.86\,\mu\text{m}$. In addition, noisy bands were removed, leading to 103 and102 channels for the Pavia University and Centre images, respectively. The Pavia University dataset is composed of 610×340 pixels and a total of 42 776 pixels for testing the classifiers. With respect to the Pavia Centre image (1096×715 pixels), the available test samples are148 152 in pixels.

The DC dataset was collected by HYDICE sensor in August 1995 over the Washington, DC Mall, which originally contained 210 bands within the 0.4–2.4 μm region. Noisy channels due to water absorption were removed, resulting in 191 spectral channels. The image contains 1280×307 pixels, with a total of 19 332 pixels available for testing the classifiers.

The number of available test samples for each dataset is given in Table IV. The number of the training samples for each class of ROSIS and HYDICE data is 150 and 100, respectively. The training samples are generated randomly from the reference. The false color images and reference maps of the test datasets are displayed in Fig. 2.

The parameter settings are listed below.

1) *The morphological filters*: EMPs were calculated using a disk SE and their radius range from 2 to 8 with step size of 1 pixel. The parameters of the EAPs were defined according to [15]: 1) area of the regions ($\lambda_a = [\,100 \quad 500 \quad 1000 \quad 5000\,]$); 2) length of the diagonal of the box bounding the region ($\lambda_d = [\,10 \quad 25 \quad 50 \quad 100\,]$); 3) first moment of inertia ($\lambda_i = [\,0.2 \quad 0.3 \quad 0.4 \quad 0.5\,]$); and 4) standard deviation of the gray-level values of the pixels in the regions ($\lambda_s = [\,20 \quad 30 \quad 40 \quad 50\,]$).

TABLE IV
Test Samples for the Three Datasets

University	Number	Centre	Number	DC Mall	Number
Trees	2064	Water	65 971	Roads	3334
Asphalt	6631	Tree	7598	Grass	3075
Bitumen	1330	Asphalts	9248	Water	2882
Gravel	2099	Bricks	2685	Trails	1034
Metal sheets	1345	Bitumen	7287	Trees	2047
Shadow	947	Tiles	42 826	Shadow	1093
Bricks	3682	Shadow	2863	Roofs	5867
Meadows	18 649	Meadows	3090		
Bare soil	5029	Bare soil	6584		
Total	42 776	**Total**	148 152	**Total**	19 332

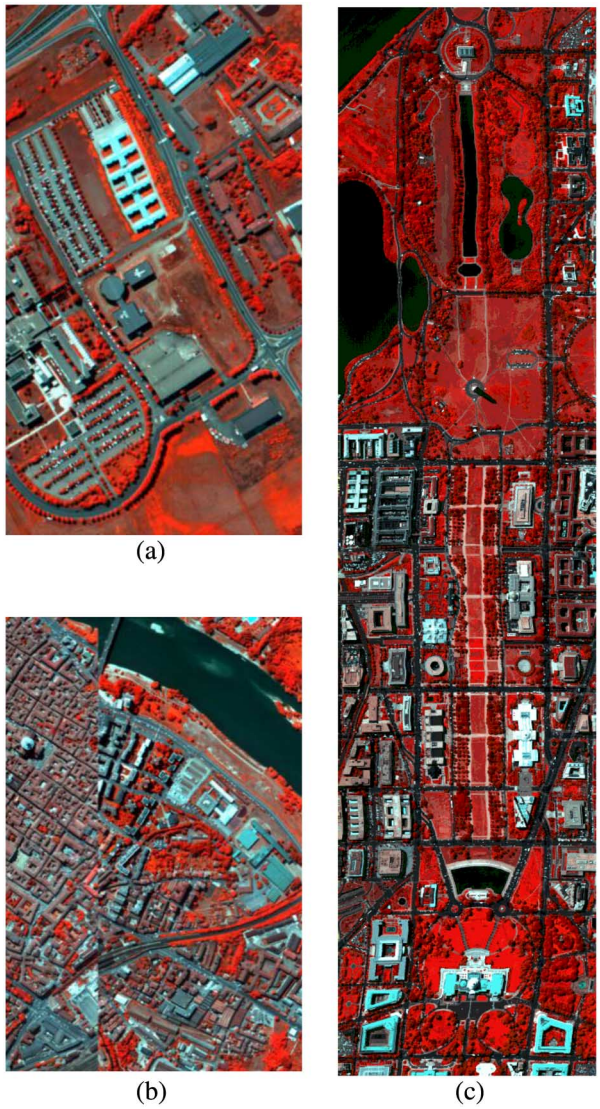

Fig. 2. (a) False color image for the University Area dataset. (b) False color image for the Pavia Centre dataset. (c) False color image for the Washington DC dataset.

TABLE V
CLASS-SPECIFIC ACCURACIES (%) OF EMPS FOR THE UNIVERSITY AREA DATASET

Accuracy	Raw	PCA	JADE-ICA	Fast-ICA	CNMF	FA	KPCA	KNMF	LPP	NPE	MPCA
AA	72.9	84.8	**84.9**	**85.2**	82.9	80.4	80.6	79.8	82.5	81.0	83.8
OA	69.9	87.7	**87.8**	**87.9**	84.5	82.4	83.4	84.1	83.3	81.4	84.5
KAPPA	63.0	83.8	**83.9**	**84.0**	79.3	76.9	77.9	79.1	78.0	75.7	79.4
Trees	63.8	88.7	88.5	88.4	84.2	72.8	76.7	76.4	78.7	84.4	82.5
Asphalt	87.7	94.4	94.4	94.3	95.7	94.1	91.8	91.6	89.2	90.6	94.8
Bitumen	61.0	83.2	83.1	84.1	80.2	75.8	78.4	81.1	63.5	56.9	92.7
Gravel	53.4	54.8	55.4	57.1	51.9	48.6	48.2	41.9	87.6	84.7	40.0
Metal sheet	92.1	92.8	92.9	93.1	94.0	95.0	86.8	80.8	96.9	99.8	93.6
Shadow	96.9	100.0	99.9	99.9	99.5	99.8	99.2	97.0	98.8	98.2	100
Bricks	66.9	68.0	68.0	67.7	66.2	67.0	74.1	74.3	56.3	61.0	74.0
Meadows	94.2	94.6	94.6	94.5	89.4	89.9	89.5	93.6	92.1	90.7	90.3
Bare soil	40.4	86.6	87.0	87.4	85.2	80.5	80.6	81.4	79.7	63.0	86.2

2) *Classifier*: Considering the hyperdimensionality of MPs, linear SVM was used for classification purposes, with penalty $\mathrm{coefficient} = 1$.
3) *Base image construction*: According to [3], [5], [6], [8], and [10], four base images were here extracted from the hyperspectral images since they can achieve a tradeoff between the computational burden and classification accuracy. The RBF kernel function was adopted for the kernel-based methods. As suggested in [27],the number of iterations of MPCA was set to 1.
4) *Accuracy assessment*: In experiments, the overall accuracy (OA), the average accuracy (AA), and the kappa coefficient (Kappa) computed from the confusion matrix are used to quantitatively evaluate the classification accuracies. It should be noted that all the experiments were repeated ten times with different starting training sets and the average accuracies are reported in Tables V–X.

B. Comparison of Methodologies for Extracting Base Images

In this section, a comparative analysis is conducted among the MPs derived from different base images.

1) Pavia University Area: The SVM classification results of EMPs and EAPs for the University Area are reported in Tables V and VI, respectively. The classification maps of different features are shown in Fig. 3. For this dataset, the raw spectral-based classification has problems in correctly classifying the nine information classes, resulting in an overall accuracy of 69.9%. In particular, very low accuracies were obtained for Trees (63.8%), Gravel (53.4%), and Bare soil (40.4%). The exploitation of either EMPs or EAPs for classification can significantly improve the results regardless of the specific base images used. It can be seen from Tables V and VI that PCA is not always the optimal strategy to generate the base images. In the case of EMPs, for instance, JADE-ICA and Fast-ICA gave better results than PCA in terms of average accuracies (AA). With respect to the case of EAPs, the JADE-ICA, FA, MPCA, and LPP outperformed PCA. Note that the methods which produced results better than PCA are highlighted in bold typeface.

2) Pavia Centre: The classification results of the EMPs and EAPs for the Pavia Centre are reported in Tables VII and VIII, respectively. Classification maps of different feature combinations are shown in Fig. 4. For this dataset, the traditional spectral classification yields satisfactory accuracies: $\mathrm{OA} = 96.9\%$, $\mathrm{AA} = 90.5\%$, and $\mathrm{Kappa} = 0.96$. Similarly, the consideration of MPs into classification shows better results than the original hyperspectral classification. In the case of EMPs, JADE-ICA and Fast-ICA provided higher accuracies than PCA once again. In addition, it can be seen that CNMF, KPCA, MPCA, and LPP also outperformed PCA. In the case of EAPs, PCA seems the most appropriate base images since it gave the highest AA (96.3%) and OA (98.9%). Note that, however, Fast-ICA achieved similar results with PCA ($\mathrm{AA} = 96.3\%$ and $\mathrm{OA} = 98.8\%$).

3) Washington DC: The classification results for the HYDICEDC data are reported in Tables IX and X, with classification maps shown in Fig. 5. The pixelwise classification accuracies based on the original hyperspectral image are $\mathrm{OA} = 88.4\%$, $\mathrm{AA} = 84.9\%$, and $\mathrm{Kappa} = 0.86$. Similarly, the original spectral classification was substantially improved by taking the morphological profiles into account, especially for the classes of roads, trails, and shadows. In the EMPs-based classification, the highest accuracy was achieved by the MPCA ($\mathrm{AA} = 98.9\%$), while PCA ranked the second place, followed by KPCA and Fast-ICA. As for the EAPs-based experiment, the JADE-ICA and Fast-ICA provided the best results in terms of quantitative accuracies, followed by the MPCA. Furthermore, FA, KNMF, and NPE outperformed the PCA base images.

The percentage of improvement for the AA obtained by the MPs-based classification compared to the raw spectral-based classification is shown in Fig. 6 for a visual comparison. The performance of the different methods considered in this study to extract base images is generally summarized in Table XI, where the base image construction methods which outperformed PCA in terms of AA in experiments are underlined using the symbol "$\surd$." It is interesting to see that the JADE-ICA and MPCA, used to produce base images for MPs, achieved better classification results than PCA in four of the six experiments. In addition, the Fast-ICA gave comparable results since it outperformed PCA in half of the experiments. Moreover, in order to further investigate their performance,

TABLE VI
CLASS-SPECIFIC ACCURACIES (%) OF EAPS FOR THE UNIVERSITY AREA DATASET

Accuracy	Raw	PCA	JADE-ICA	Fast-ICA	CNMF	FA	KPCA	KNMF	LPP	NPE	MPCA
AA	72.9	94.4	**95.8**	92.7	94.3	**95.3**	93.9	93.2	**94.8**	92.2	**94.8**
OA	69.9	95.9	**96.8**	93.1	95.4	**95.8**	94.1	92.3	**96.1**	92.6	**95.5**
KAPPA	63.0	94.6	**95.7**	90.9	94.0	**94.5**	92.3	89.9	**94.9**	90.2	**94.1**
Trees	63.8	78.1	79.3	81.5	73.6	77.7	73.7	65.6	84.2	80.3	78.7
Asphalt	87.7	99.2	99.3	96.7	99.4	99.3	98.5	98.8	98.4	93.5	99.2
Bitumen	61.0	99.9	99.9	93.5	99.8	100.0	99.9	100.0	99.1	88.0	100.0
Gravel	53.4	88.2	97.0	89.9	92.3	94.5	94.6	95.4	95.5	90.0	91.2
Metal sheet	92.1	95.9	96.1	99.4	97.3	98.2	96.9	98.0	96.6	99.8	95.4
Shadow	96.9	99.9	99.5	99.8	99.4	99.7	99.8	99.7	97.4	99.9	99.9
Bricks	66.9	90.3	91.8	83.2	88.6	91.3	86.0	89.4	82.8	84.8	91.0
Meadows	94.2	99.4	99.6	95.8	99.6	98.1	96.7	94.5	99.8	95.3	97.8
Bare soil	40.4	99.1	99.3	94.6	98.8	99.2	99.3	97.6	99.1	98.4	99.7

TABLE VII
CLASS-SPECIFIC ACCURACIES (%) OF EMPS FOR THE PAVIA CENTRE DATASET

Accuracy	Raw	PCA	JADE-ICA	Fast-ICA	CNMF	FA	KPCA	KNMF	LPP	NPE	MPCA
AA	90.5	93.4	**94.6**	**94.7**	**94.1**	93.2	**93.8**	90.9	**94.0**	92.0	**95.0**
OA	96.9	97.8	**98.0**	**98.4**	**97.5**	97.7	**97.9**	96.6	**97.9**	97.3	**98.2**
KAPPA	95.6	96.9	**97.2**	**97.7**	**96.4**	96.7	**97.0**	95.2	**97.0**	96.2	**97.4**
Water	100.0	100.0	100.0	100.0	100.0	100.0	100.0	100.0	99.8	99.9	99.9
Trees	97.9	98.4	98.5	97.2	99.2	98.8	98.7	97.7	96.7	98.8	98.0
Asphalt	87.4	88.7	87.9	95.5	78.6	87.9	87.5	80.2	92.3	85.1	89.1
Bricks	65.5	84.7	91.5	89.1	87.0	85.7	79.0	82.3	78.8	77.8	95.1
Bitumen	86.6	91.4	92.5	91.4	96.1	91.1	91.2	92.4	94.6	90.3	96.5
Tiles	99.8	99.9	99.8	100.0	99.9	99.8	100.0	99.7	99.4	99.8	100.0
Shadow	100..0	100.0	99.9	98.5	99.9	99.9	100.0	100.0	99.6	90.0	100.0
Meadows	83.3	82.1	83.2	83.3	89.6	80.2	92.1	71.8	89.6	91.1	81.0
Bare soil	94.2	95.7	98.4	97.2	96.9	95.1	95.7	93.9	95.2	95.2	95.4

TABLE VIII
CLASS-SPECIFIC ACCURACIES (%) OF EAPS FOR THE PAVIA CENTRE DATASET

Accuracy	Raw	PCA	JADE-ICA	Fast-ICA	CNMF	FA	KPCA	KNMF	LPP	NPE	MPCA
AA	90.5	96.3	95.4	96.3	96.1	95.6	92.0	93.9	96.0	93.3	95.9
OA	96.9	98.9	98.6	98.8	98.6	98.2	96.8	97.3	98.0	96.9	98.4
KAPPA	95.6	98.5	98.0	98.3	98.0	97.5	95.6	96.2	97.2	95.6	97.8
Water	100.0	100.0	100.0	100.0	99.9	99.8	99.8	99.9	99.7	99.5	100.0
Trees	97.9	98.3	98.0	97.9	97.4	97.7	97.2	97.6	97.9	98.7	98.5
Asphalt	87.4	96.2	94.6	93.0	91.6	87.5	87.4	79.8	93.9	75.9	88.6
Bricks	65.5	95.1	94.4	97.0	97.1	98.0	90.7	98.6	94.0	94.8	99.1
Bitumen	86.6	98.8	97.5	98.9	98.4	98.6	94.2	97.3	99.1	94.3	97.2
Tiles	99.8	99.9	99.9	99.9	99.9	99.9	98.9	99.9	97.6	99.9	99.9
Shadow	100..0	100.0	100.0	99.9	100.0	100.0	100.0	100.0	99.6	89.3	100.0
Meadows	83.3	78.7	75.1	80.9	81.3	79.0	65.4	72.8	83.3	88.8	80.1
Bare soil	94.2	99.6	99.2	99.5	99.4	99.6	94.8	99.2	98.5	98.8	99.3

all the base images are ranked from one to ten in terms of their accuracies achieved in the six experiments, and the final score (Table XI) is computed as the average ranking in all the tests. Accordingly, a smaller ranking score infers that this base image is more appropriate for MPs-based image classification. Table XI shows that the top three base images are MPCA (score $= 2.8$), Fast-ICA (score $= 3.2$), JADE-ICA (score $= 3.3$), respectively, significantly outperforming PCA (score $= 4.2$). In addition, the average AA for each method across different datasets is reported in the table. Similarly, the

TABLE IX
CLASS-SPECIFIC ACCURACIES (%) OF EMPS FOR THE WASHINGTON DC DATASET

Accuracy	Raw	PCA	JADE-ICA	Fast-ICA	CNMF	FA	KPCA	KNMF	LPP	NPE	MPCA
AA	84.9	98.5	97.2	97.8	97.0	97.1	97.9	95.2	96.4	96.5	**98.9**
OA	88.4	98.7	98.1	98.0	98.0	98.1	98.3	96.8	96.8	95.3	**98.9**
KAPPA	86.0	98.4	97.6	97.5	97.6	97.7	98.0	96.1	96.1	95.4	**98.7**
Roads	87.6	98.1	97.5	93.5	99.4	97.0	97.1	94.4	90.3	97.1	97.7
Grass	97.1	98.5	98.1	98.7	99.0	98.9	98.4	99.8	97.8	97.9	98.8
Water	99.1	100.0	100.0	100.0	100.0	100.0	100.0	100.0	100.0	99.6	100.0
Trails	50.1	96.0	89.6	94.8	94.8	92.0	92.9	76.2	94.6	93.2	99.6
Trees	96.2	99.0	99.0	99.7	97.7	99.9	99.3	100	99.6	96.3	98.0
Shadows	66.5	99.5	97.8	98.7	90.0	93.0	98.8	96.7	93.8	93.4	98.4
Roofs	97.7	98.8	98.8	99.2	98.1	99.0	98.8	99.0	98.7	98.2	99.4

TABLE X
CLASS-SPECIFIC ACCURACIES (%) OF EAPS FOR THE WASHINGTON DC DATASET

Accuracy	Raw	PCA	JADE-ICA	Fast-ICA	CNMF	FA	KPCA	KNMF	LPP	NPE	MPCA
AA	84.9	95.5	**97.2**	**97.5**	93.1	**95.9**	95.3	**96.6**	94.0	**95.6**	**96.8**
OA	88.4	97.3	**98.1**	**98.3**	95.6	**97.6**	96.8	**97.7**	96.4	**97.1**	**98.0**
KAPPA	86.0	96.7	**97.7**	**98.0**	94.6	**97.0**	96.1	**97.2**	95.6	**96.4**	**97.6**
Roads	87.6	97.9	97.5	98.4	99.6	97.9	95.4	98.9	97.4	98.2	97.7
Grass	97.1	98.5	97.6	98.9	98.8	98.4	97.4	98.2	97.5	99.6	98.8
Water	99.1	100.0	100.0	100.0	100.0	100.0	100.0	100.0	100.0	100.0	100.0
Trails	50.1	85.0	93.0	93.3	69.8	84.6	88.3	93.7	74.5	89.3	89.5
Trees	96.2	98.7	99.6	98.7	94.2	99.3	98.1	96.5	99.6	92.0	97.6
Shadows	66.5	89.6	93.8	94.2	92.0	92.1	89.4	90.7	89.9	91.9	94.6
Roofs	97.7	98.8	99.2	98.8	97.5	99.0	98.7	98.3	99.0	98.2	99.3

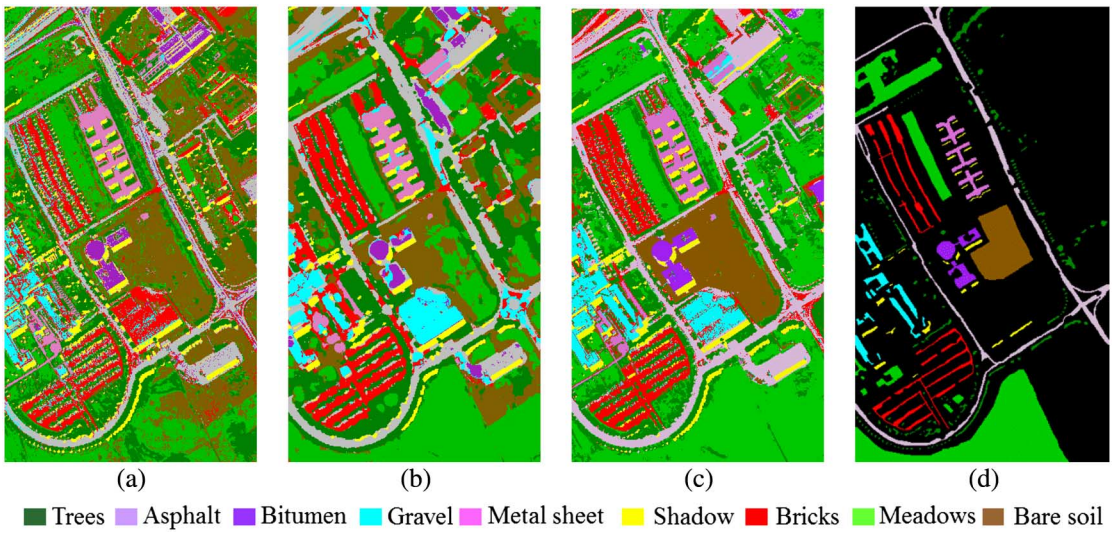

Fig. 3. SVM classification results for (a) the 103-D hyperspectral image of University area; (b) Fast − ICA + EMPs; (c) JADE − ICA + EAPs; and (d) the ground truth map.

MPCA obtains the highest accuracy (94.20%), followed by JADE-ICA (94.18%) and Fast-ICA (94.03%), which outperform PCA (93.82%).

Traditional base images are extracted from the original hyperspectral space in a vector-based manner, with each vector representing the spectral information at a certain location. Such methods do not effectively take advantage of the spectral–spatial correlation between neighboring pixels. However, the multilinear PCA, which aims to process the hyperspectral image as a cube (third-order tensor), is more capable of representing the spectral–spatial information in the original data. As revealed in this experiment, MPCA is the optimal approach for generating base images of the MPs for the subsequent spectral–spatial classification. In addition, it is

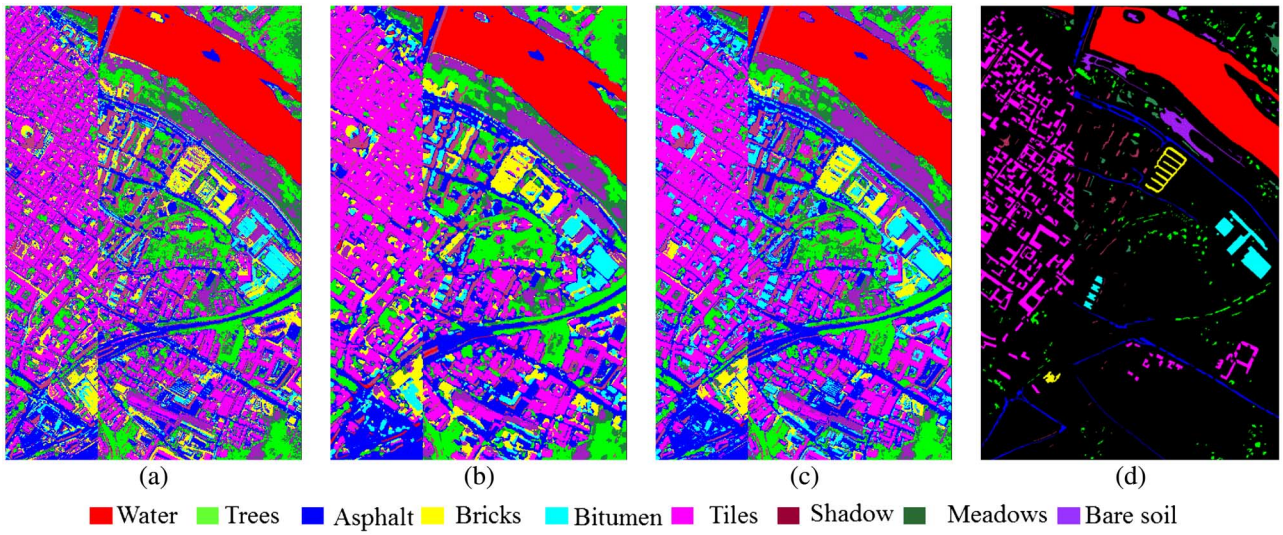

Fig. 4. SVM classification results for (a) the 103-D hyperspectral image of University area; (b) Fast − ICA + EMPs; (c) PCA + EAPs; and (d) the ground truth map.

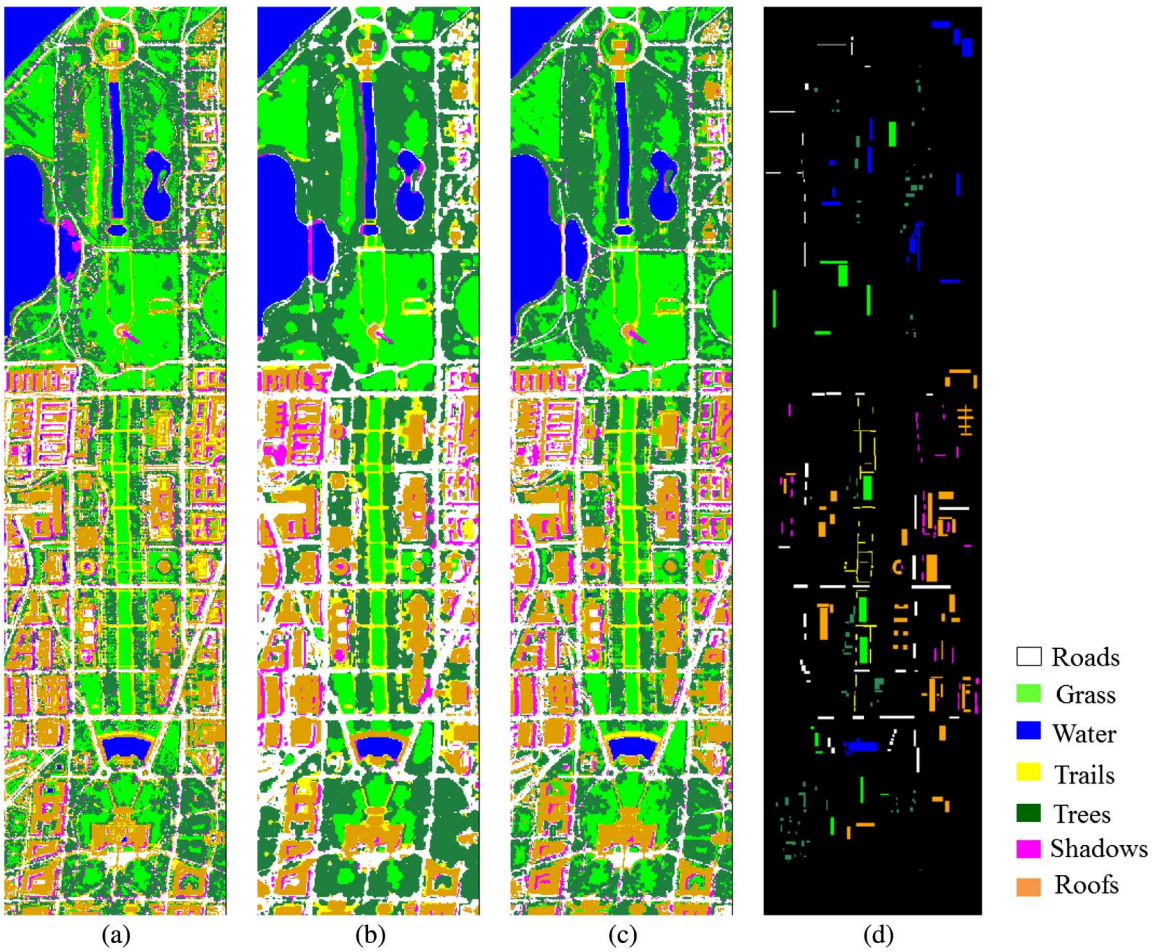

Fig. 5. SVM classification results for (a) the 103-D hyperspectral image of University area; (b) MPCA + EMPs; (c) Fast − ICA + EAPs; and (d) the ground truth map.

found that ICA methods are more appropriate than PCA for producing base images. This phenomenon can be attributed to the fact that ICA, making use of statistical independency as a criterion to separate components, has a potential for avoiding the information loss in the PCA transformation. As for the manifold leaning, it is shown that LPP is better than NPE in terms of the classification accuracies and the ranking scores, but generally speaking, they did not achieve comparable results

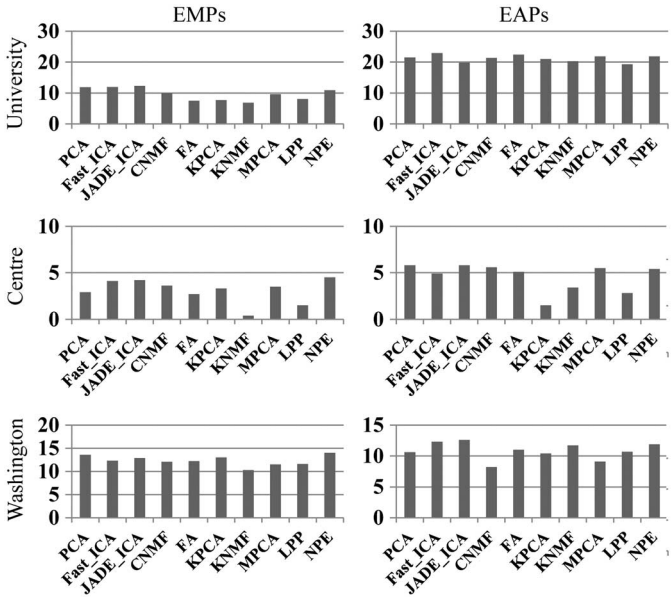

Fig. 6. Percentage of improvement for the AA obtained by the MPs(APs)-based classification methods compared to the raw spectral-based method.

to PCA. This result can be attributed to the fact that, in most cases, the intrinsic dimensionality of the data is very high [54]. Consequently, the manifold transformation could not provide better results than PCA with low-dimensional base images.

C. Impact of the Number of Training Samples

In order to investigate the impact of the number of training samples to the classification, four groups of training samples are used in the University dataset: 25, 50, 75, and 150 pixels for each class. The classification accuracies based on different base images, as a function of the number of samples, are compared in Fig. 7. In general, the accuracies are relatively insensitive to the number of training samples, especially for the EAPs. It can be observed that the MPCA as well as the ICA achieve high accuracies in most of the cases regardless of the number of training samples. This is consistent with the results in the aforementioned experiments.

D. Analysis of MMPs

The accuracies of MMPs are provided in Table XII. The three most effective methods for extracting base images (MPCA, JADE-ICA, and Fast-ICA) and their respective MPs were used to build the MMPs. From the table, it can be seen that the performance of the MMPs is dependent on the morphological features used.

In the case of the decision fusion of EMPs, the MMPs did not produce better results than the best available individual base images. For instance, the AA decreased by about 0.6% and 2.4% in average for the Pavia University and Washington datasets, respectively. However, the situation is quite different in the case of EAPs, where the accuracies obtained by MMPs were higher than those obtained by the best available base images, and the improvements in terms of AA were 1.9%, 2.2%, and 1.1% on average, respectively, for the Pavia University, Centre, and Washington datasets. Considering the fact that the classification accuracies based on individual MPs are already quite high, the accuracy increments obtained by the MMPs are promising. With respect to the fusion methods, it is shown that the probability and uncertainty algorithms are better than the majority voting methods.

Considering the stacked MMPs, it can be seen that the accuracies obtained by the EAPs are also higher than the accuracies obtained by the EMPs in all the experiments. It can be stated that the EAPs show much better discriminative ability than EMPs for hyperspectral urban classification. Accordingly, the analysis here focuses on the EAPs. In general, the LORSAL classifier outperforms the linear SVM in all the three datasets for interpreting the MMPs, which verifies the efficiency of the LORSAL classifier for processing hyperdimensional data.

Generally speaking, the MMPs based on the EMPs gave similar accuracies as those achieved by the best available base images. The MMPs based on the EAPs, however, provided better or comparable results than the EAPs extracted from individual base images. Both decision fusion and stacked strategies are effective in synthesizing and classifying the hyperdimensional feature of MMPs. In particular, it is found that the sparse multinomial logistic regression optimized with the LORSAL algorithm is a very efficient scheme for classifying the MMPs.

E. Comparisons

In this paper, our focus is mainly on the use of unsupervised FE strategies for generating base images for MPs. A particular feature of such unsupervised methods is that they are data-driven and self-adaptive. On the other hand, however, the effectiveness of supervised FE methods highly relies on the chosen samples. Moreover, supervised methods tend to significantly increase the feature dimensionality of the MPs, since the commonly used supervised FE methods, e.g., DAFE (discriminant analysis feature extraction), DBFE (decision boundary feature extraction), and NWFE (nonparametric weighted feature extraction) [55], need approximately 20 base images to effectively represent a hyperspectral image. This will lead to a hyperdimensional and redundant MPs feature space. Instead, with respect to the unsupervised methods, it is found that only four base images are generally effective for building the MPs.

In Table XIII, we compare the performance of unsupervised and supervised FE methods as base images for classification based on EAPs. Readers can refer to [55] for a detailed explanation of the parameter settings for the supervised methods. It is shown that some unsupervised FE methods have the potential to provide better results than the supervised ones. In addition, the MMPs constructed on the multicomponent base images can further increase the classification accuracy by about 3%. It should be kept in mind that a large amount of training samples are needed for the supervised methods, while the unsupervised ones are carried out automatically and are adaptive to the specific image data. The supervised strategies may be less effective in many practical scenarios (especially when dealing with large datasets), since the labeled samples might not be sufficient for properly and completely modeling the heterogeneity of the data [55].

TABLE XI
GENERAL COMPARISON OF BASE IMAGE CONSTRUCTION METHODS

Base images		University		Centre		Washington DC		Score (PCA = 4.2)	Averaged AA
		EMPs	EAPs	EMPs	EAPs	EMPs	EAPs		
Linear	JADE-ICA	√	√	√			√	3.3	94.18
	Fast-ICA	√		√			√	3.2	94.03
	CNMF			√				5.8	92.92
	FA		√				√	6.0	92.92
Nonlinear	KPCA			√				7.0	92.25
	KNMF						√	8.3	91.60
Multilinear	MPCA		√	√		√	√	**2.8**	94.20
Manifold	LPP		√	√				6.2	91.76
Learning	NPE						√	8.2	92.95

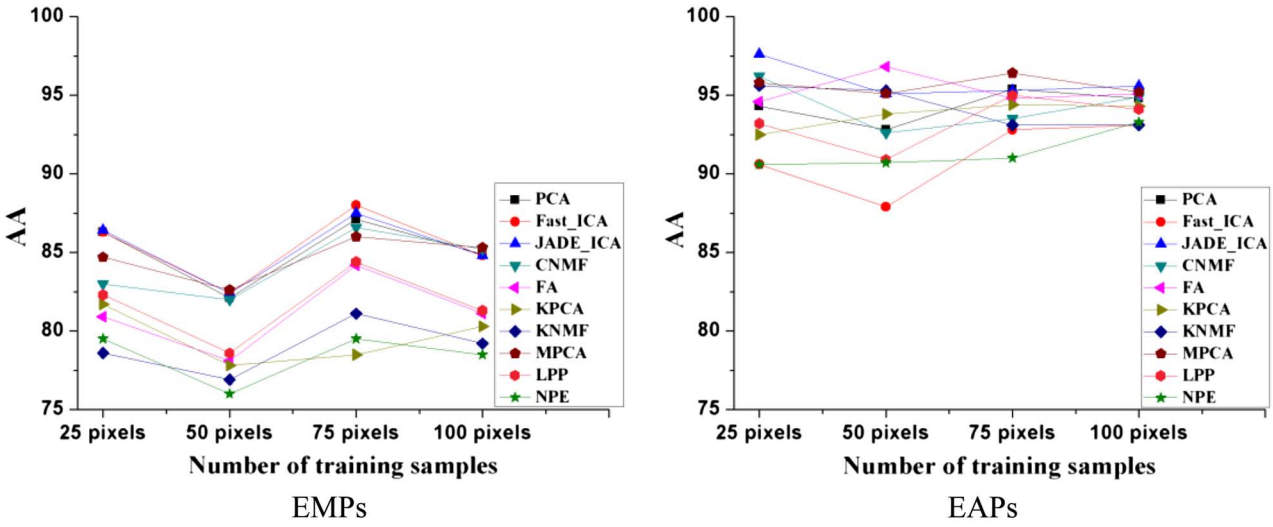

Fig. 7. Classification accuracies (in percentage) for different training sample sizes (Pavia University dataset).

TABLE XII
ACCURACIES OF MMPS FOR THE THREE HYPERSPECTRAL DATASETS ("OPTIMAL" INDICATES THE ACCURACIES OBTAINED BY THE BEST AVAILABLE BASE IMAGES)

		EMPs						EAPs					
			Decision fusion			Stacked			Decision fusion			Stacked	
		Optimal	Voting	Probability	Uncertainty	L-SVM	LORSAL	Optimal	Voting	Probability	Uncertainty	L-SVM	LORSAL
University	AA	85.2	84.4	84.7	84.7	85.6	84.3	95.8	97.5	97.8	97.7	96.8	98.2
	OA	87.9	88.0	88.0	87.8	85.0	87.2	96.8	97.0	97.4	97.4	97.6	98.6
Centre	AA	95.0	95.4	95.8	95.9	95.6	94.4	96.3	98.4	98.5	98.5	97.0	97.7
	OA	98.2	98.0	98.2	98.2	98.2	97.7	98.9	99.1	99.0	99.0	99.0	98.8
Washington	AA	98.9	96.0	96.7	96.8	98.1	97.8	97.5	98.5	98.6	98.6	97.6	98.5
	OA	98.9	98.2	98.4	98.4	97.9	96.7	98.3	99.1	99.1	99.0	97.8	98.4

TABLE XIII
COMPARISON BETWEEN UNSUPERVISED AND SUPERVISED FE METHODS FOR PRODUCING THE BASE IMAGES FOR EAPS USING THE PAVIA UNIVERSITY DATASET

	Supervised [55]			Unsupervised				MMPs	
	DAFE	DBFE	NWFE	JADE-ICA	FA	LPP	MPCA	DF	LORSAL
AA	95.6	92.6	93.6	95.8	95.3	94.8	94.8	97.8	98.2
OA	96.6	91.6	89.2	96.8	95.8	96.1	95.5	97.4	98.6

VI. Conclusion and Future Lines

In this study, a systematic investigation of techniques for producing base images for the construction of morphological profiles is conducted, and a novel technique based on MMPs extracted from multicomponent base images is proposed. The main contributions of this work can be summarized as follows.

1) A systematic study of different techniques for the construction of base images for MPs was carried out, including methods that were never considered for this purpose in previous developments. Specifically, we considered methods in four categories: linear, nonlinear, manifold learning, and multilinear transformations. For instance, the multilinear PCA and manifold learning algorithms are used for the first time in this work to generate base images for MPs.
2) A new concept of MMPs was proposed for integrating the MPs derived from multiple base images since the multicomponent base images have the potential to provide more effective spectral–spatial representations for hyperspectral images. This multicomponent framework represents a unique contribution of this work.

Extensive experiments were performed using three widely used hyperspectral images with high-spatial resolution. Some important observations resulting from our study can be summarized as follows.

1) The MPCA, a tensor-based feature representation approach, is the most suitable strategy for generating base images in terms of classification accuracies because it is able to effectively model the spectral–spatial correlation between neighboring pixels.
2) The ICA-based algorithms (JADE-ICA and Fast-ICA in this study) are also more effective in producing base images in terms of accuracies than the traditional strategy, i.e., PCA.
3) Manifold learning methods did not outperform PCA in our experiments, mainly because they need higher dimensionality of the feature space to represent the data manifold for hyperspectral images of complex scenes.
4) The proposed MMPs can further improve the classification accuracy as compared to the result achieved by the most effective base images when using EAPs. Moreover, the decision fusion and stacking strategies are effective for integrating the information of MMPs for hyperspectral image classification. In particular, the proposed LORSAL-based sparse classifier can efficiently classify the hyperdimensional space of MMPs.

In summary, it can be concluded that the newly introduced MMP represents a promising method for MPs-based hyperspectral image classification. In the future, we plan to discuss the influence of different base images for other spectral–spatial classification, e.g., texture or object-based methods, as well as to develop computationally efficient implementations of the newly developed approaches using high-performance computing architectures.

Acknowledgment

The authors would like to acknowledge Prof. P. Gamba, University of Pavia, Italy, for providing the ROSIS data and Prof. D. A. Landgrebe, Purdue University, USA, for providing the HYDICE dataset. The authors also gratefully appreciate the insightful suggestions from the anonymous reviewers, which significantly improved the quality of this paper.

References

[1] M. Fauvel, Y. Tarabalka, J. A. Benediktsson, J. Chanussot, and J. C. Tilton, "Advances in spectral–spatial classification of hyperspectral images," *Proc. IEEE*, vol. 101, no. 3, pp. 652–675, Mar. 2013.

[2] M. Pesaresi and J. Benediktsson, "A new approach for the morphological segmentation of high resolution satellite imagery," *IEEE Trans. Geosci. Remote Sens.*, vol. 39, no. 2, pp. 309–320, Feb. 2001.

[3] J. A. Benediktsson, J. A. Palmason, and J. Sveinsson, "Classification of hyperspectral data from urban areas based on extended morphological profiles," *IEEE Trans. Geosci. Remote Sens.*, vol. 43, no. 3, pp. 480–491, Mar. 2005.

[4] X. Huang, L. Zhang, and L. Wang, "Evaluation of morphological texture features for mangrove forest mapping and species discrimination using multispectral IKONOS imagery," *IEEE Geosci. Remote Sens. Lett.*, vol. 6, no. 3, pp. 393–397, Jul. 2009.

[5] X. Huang and L. Zhang, "Road centreline extraction from high-resolution imagery based on multiscale structural features and support vector machines," *Int. J. Remote Sens.*, vol. 30, no. 8, pp. 1977–1987, Apr. 2009.

[6] M. Fauvel, J. A. Benediktsson, J. Chanussot, and J. R. Sveinsson, "Spectral and spatial classification of hyperspectral data using SVMs and morphological profiles," *IEEE Trans. Geosci. Remote Sens.*, vol. 46, no. 11, pp. 3804–3814, Nov. 2008.

[7] M. Dalla Mura, J. A. Benediktsson, B. Waske, and L. Bruzzone, "Morphological attribute profiles for the analysis of very high resolution images," *IEEE Trans. Geosci. Remote Sens.*, vol. 48, no. 10, pp. 3747–3762, Oct. 2010.

[8] M. Dalla Mura, J. A. Benediktsson, B. Waske, and L. Bruzzone, "Extended profiles with morphological attribute filters for the analysis of hyperspectral data," *Int. J. Remote Sens.*, vol. 31, no. 22, pp. 5975–5991, Nov. 2010.

[9] W. Liao, R. Bellens, A. Pizurica, W. Philips, and Y. Pi, "Classification of hyperspectral data over urban areas using directional morphological profiles and semi-supervised feature extraction," *IEEE J. Sel. Topics Appl. Earth Observ. Remote Sens.*, vol. 5, no. 3, pp. 1164–1176, Aug. 2012.

[10] X. Huang and L. Zhang, "An SVM ensemble approach combining spectral, structural, and semantic features for the classification of high resolution remotely sensed imagery," *IEEE Trans. Geosci. Remote Sens.*, vol. 51, no. 1, pp. 257–272, Jan. 2013.

[11] K. Tan, E. Li, Q. Du, and P. Du, "Hyperspectral image classification using band selection and morphological profiles," *IEEE J. Sel. Topics Appl. Earth Observ. Remote Sens.*, vol. 7, no. 1, pp. 40–48, Jan. 2014, doi: 10.1109/JSTARS.2013.2265697.

[12] M. Fauvel, J. Chanussot, and J. A. Benediktsson, "Kernel principal component analysis for the classification of hyperspectral remote-sensing data over urban areas," *EURASIP J. Adv. Signal Process.*, vol. 2009, pp. 1–14, Feb. 2009.

[13] J. A. Palmason, J. A. Benediktsson, J. R. Sveinsson, and J. Chanussot, "Classification of hyperspectral data from urban areas using morphological preprocessing and independent component analysis," in *Proc. IEEE Trans. Int. Geosci. Remote Sens.*, Jul. 2005, vol. 1, pp. 176–179.

[14] J. A. Palmason, "Classification of hyperspectral data from urban areas," M.S. thesis, Fac. Eng., Univ. Iceland, Reykjavik, Iceland, 2005.

[15] M. Dalla Mura, A. Villa, J. A. Benediktsson, J. Chanussot, and L. Bruzzone, "Classification of hyperspectral images by using extended morphological attribute profiles and independent component analysis," *IEEE Geosci. Remote Sens. Lett.*, vol. 8, no. 3, pp. 542–546, May 2011.

[16] P. R. Marpu, M. Pedergnana, M. Dalla Mura, J. A. Benediktsson, and L. Bruzzone, "Automatic generation of standard deviation attribute profiles for spectral–spatial classification of remote sensing data," *IEEE Geosci. Remote Sens. Lett.*, vol. 10, no. 2, pp. 293–297, Mar. 2013.

[17] H. Lu, K. N. Plataniotis, and A. N. Venetsanopoulos, "Multilinear principal component analysis of tensor objects for recognition," in *Proc. Int. Conf. Pattern Recognit.*, Aug. 2006, pp. 776–779.

[18] J. Zhang, S. Z. Li, and J. Wang, "Manifold learning and applications in recognition," in *Intelligent Multimedia Processing With Soft Computing*. Berlin, Germany: Springer-Verlag, 2004, pp. 281–300.

[19] A. Hyvarinen, "Fast independent component analysis with noisy data using Gaussian moments," in *Proc. Int. Symp. Circuits Syst.*, May 1999, pp. 57–61.

[20] N. Wang, B. Du, and L. Zhang, "An endmember dissimilarity constrained non-negative matrix fractorization method for hyperspectral unmixing," *IEEE J. Sel. Topics Appl. Earth Observ.* Remote Sens., vol. 6, no. 2, pp. 554–569, Apr. 2013.
[21] M. Tipping and C. Bishop, "Probabilistic principal component analysis," Aston Univ., Birmingham, U.K., Tech. Rep. NCRG/97/010, Sep. 1997.
[22] L. Ma, M. M. Crawford, and J. Tian, "Local manifold learning-based k-nearest-neighbor for hyperspectral image classification," *IEEE Trans. Geosci. Remote Sens.*, vol. 48, no. 11, pp. 4099–4109, Nov. 2010.
[23] D. Zhang, Z. Zhou, and S. Chen, "Non-negative matrix factorization on Kernels," in *Proc. Pacific Rim Int. Conf. Artif. Intell.*, Guilin, China, 2006, pp. 404–412.
[24] C. Bachmann, T. Ainsworth, and R. Fusina, "Exploiting manifold geometry in hyperspectral imagery," *IEEE Trans. Geosci. Remote Sens.*, vol. 43, no. 3, pp. 441–454, Mar. 2005.
[25] X. He and P. Niyogi, "Locality preserving projections," in *Proc. Conf. Adv. Neural Inf. Process. Syst. (NIPS'03)*, Vancouver, Canada, 2003, vol. 16, pp. 234–241.
[26] X. He, D. Cai, S. Yan, and H.-J. Zhang, "Neighborhood preserving embedding," in *Proc. IEEE Int. Conf. Comput. Vis.*, 2005, pp. 1208–1213.
[27] H. Lu, K. Plataniotis, and A. Venetsanopoulos, "MPCA: Multilinear principal component analysis of tensor objects," *IEEE Trans. Neural Netw.*, vol. 19, no. 1, pp. 18–39, Jan. 2008.
[28] R.-E. Fan, K.-W. Chang, C.-J. Hsieh, X.-R. Wang, and C.-J. Lin, "LIBLINEAR: A library for large linear classification," *J. Mach. Learn. Res.*, vol. 9, pp. 1871–1874, 2008.
[29] J. Bioucas-Dias and M. Figueiredo, "Logistic regression via variable splitting and augmented Lagrangian tools," Instituto Superior Técnico, TULisbon, Lisbon, Portugal, Tech. Rep., 2009.
[30] P. Soille, *Morphological Image Analysis*. Berlin, Germany: Springer-Verlag, 1999.
[31] L. Vincent, "Morphological grayscale reconstruction in image analysis," *IEEE Trans. Image Process.*, vol. 2, no. 2, pp. 176–201, Apr. 1993.
[32] D. Tuia, F. Pacifici, M. Kanevski, and W. Emery, "Classification of very high spatial resolution imagery using mathematical morphology and support vector machines," *IEEE Trans. Geosci. Remote Sens.*, vol. 47, no. 11, pp. 3866–3879, Nov. 2009.
[33] T. Castaings, B. Waske, J. A. Benediktsson, and J. Chanussot, "On the influence of feature reduction for the classification of hyperspectral images based on the extended morphological profile," *Int. J. Remote Sens.*, vol. 31, no. 22, pp. 5921–5939, Jul. 2010.
[34] E. J. Breen and R. Jones, "Attribute openings, thinnings and granulometries," *Comp. Vis. Image Understand.*, vol. 64, no. 3, pp. 377–389, Nov. 1996.
[35] L. Zhang, X. Huang, B. Huang, and P. Li, "A pixel shape index coupled with spectral information for classification of high spatial resolution remotely sensed imagery," *IEEE Trans. Geosci. Remote Sens.*, vol. 44, no. 10, pp. 2950–2961, Oct. 2006.
[36] J. F. Cardoso, "High-order contrasts for independent component analysis," *Neural Comput.*, vol. 11, no. 1, pp. 157–192, Jan. 1999.
[37] D. Lee and H. S. Seung, "Learning the parts of objects by nonnegative matrix factorization," *Nature*, vol. 401, pp. 788–791, Oct. 1999.
[38] L. D. Miao and H. R. Qi, "Endmember extraction from highly mixed data using minimum volume constrained nonnegative matrix factorization," *IEEE Trans. Geosci. Remote Sens.*, vol. 45, no. 3, pp. 765–777, Mar. 2007.
[39] X. Huang and L. Zhang, "A comparative study of spatial approaches for urban mapping using hyperspectral ROSIS images over Pavia city, northern of Italy," *Int. J. Remote Sens.*, vol. 30, no. 12, pp. 3205–3221, Jan. 2009.
[40] I. K. Fodor, "A survey of dimension reduction techniques," Lawrence Livermore Nat. Lab., Livermore, CA, USA, Tech. Rep. UCRL-ID-148494, May 2002.
[41] *Factor Analysis* [Online]. Available: http://en.wikipedia.org/wiki/Factor_analysis, accessed on Dec. 05, 2013.
[42] S. Roweis and L. Saul, "Nonlinear dimensionality reduction by locally linear embedding," *Science*, vol. 290, no. 5500, pp. 2323–2326, Dec. 2000.
[43] Z. Long, Q. Du, and N. H. Younan, "Multiscale spectral-spatial hyperspectral classification using multilinear PCA and contourlet transform," in *Proc. 5th IEEE GRSS Workshop Hyperspectral Signal Process. Evol. Remote Sens*., Gainesville, FL, USA, Jun. 2013.
[44] D. Böhning, "Multinomial logistic regression algorithm," *Ann. Inst. Stat. Math.*, vol. 44, no. 1, pp. 197–200, Mar. 1992.
[45] M. A. T. Figueiredo, "Adaptive sparseness for supervised learning," *IEEE Trans. Pattern Anal. Mach. Intell.*, vol. 25, no. 9, pp. 1150–1159, Sep. 2003.
[46] B. Krishnapuram, L. Carin, and A. Hartemink, "Joint classifier and feature optimization for cancer diagnosis using gene expression data," in *Proc. Int. Conf. Res. Comput. Mol. Biol.*, 2003, pp. 167–175.
[47] B. Krishnapuram, A. Hartemink, L. Carin, and M. Figueiredo, "A Bayesian approach to joint feature selection and classifier design," *IEEE Trans. Pattern Anal. Mach. Intell.*, vol. 26, no. 9, pp. 1105–1111, Sep. 2004.
[48] J. Borges, J. Bioucas-Dias, and A. Marçal, "Fast sparse multinomial regression applied to hyperspectral data," in *Proc. 3rd Int. Conf. Image Anal. Recognit. (ICIAR)*, 2006, pp. 700–709.
[49] J. Li, J. Bioucas-Dias, and A. Plaza, "Semi-supervised hyperspectral image segmentation using multinomial logistic regression with active learning," *IEEE Trans. Geosci. Remote Sens.*, vol. 48, no. 11, pp. 4085–4098, Nov. 2010.
[50] J. Li, J. Bioucas-Dias, and A. Plaza, "Hyperspectral image segmentation using a new Bayesian approach with active learning," *IEEE Trans. Geosci. Remote Sens.*, vol. 49, no. 10, pp. 3947–3960, Oct. 2011.
[51] X. Huang and L. Zhang, "Comparison of vector stacking, multi-SVMs fuzzy output, and multi-SVMs voting methods for multiscale VHR urban mapping," *IEEE Geosci. Remote Sens. Lett.*, vol. 7, no. 2, pp. 261–265, Apr. 2010.
[52] J. Li, J. M. Bioucas-Dias, and A. Plaza, "Semi-supervised hyperspectral image classification based on a Markov random field and sparse multinomial logistic regression," in *Proc. IEEE Int. Geosci. Remote Sens. Symp*., 2009, pp. III-817–III-820.
[53] B. Song *et al.*, "Remotely sensed image classification using sparse representations of morphological attribute profiles," *IEEE Trans. Geosci. Remote Sens.*, vol. 52, no. 8, pp. 5122–5136, Aug. 2014.
[54] L. van der Maaten, E. Postma, and J. van den Herik, "Dimensionality reduction: A comparative review," Tilburg Univ., Tilburg, The Netherlands, Tech. Rep. TiCC-TR 2009-005, 2009.
[55] P. R. Marpu *et al.*, "Classification of hyperspectral data using extended attribute profiles based on supervised and unsupervised feature extraction techniques," *Int. J. Image Data Fusion*, vol. 3, no. 3, pp. 269–298, Sep. 2012.
[56] T. Li and C. Ding, "The relationships among various nonnegative matrix factorization methods for clustering," in *Proc. IEEE Int. Conf. Data Min.*, 2006, pp. 362–371.

Xin Huang (M'13–SM'14) received the Ph.D. degree in photogrammetry and remote sensing from the State Key Laboratory of Information Engineering in Surveying, Mapping, and Remote Sensing (LIESMARS), Wuhan University, Wuhan, China, in 2009.

Currently, he is a Full Professor with the LIESMARS, Wuhan University. He has published more than 45 peer-reviewed articles in the international journals. He has frequently served as a Referee of many international journals for remote sensing. His research interests include hyperspectral data analysis, high-resolution image processing, pattern recognition, and remote sensing applications.

Dr. Huang was the recipient of the Top-Ten Academic Star of Wuhan University in 2009. In 2010, he received the Boeing Award for the best paper in image analysis and interpretation from the American Society for Photogrammetry and Remote Sensing, Bethesda, MD, USA. In 2011, he was the recipient of the New Century Excellent Talents in University from the Ministry of Education of China, Beijing, China. In 2011, he was recognized by the IEEE Geoscience and Remote Sensing Society as the Best Reviewer of IEEE GEOSCIENCE AND REMOTE SENSING LETTERS. In 2012, he was the recipient of the National Excellent Doctoral Dissertation Award of China. He was the winner of the IEEE GRSS 2014 data fusion contest. Since 2014, he serves as an Associate Editor of the IEEE GEOSCIENCE AND REMOTE SENSING LETTERS.

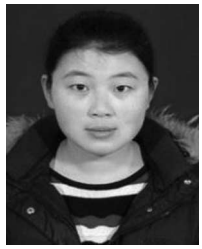

Xuehua Guan received the B.S. degree in remote sensing science and technology from Shandong University of Science and Technology, Qingdao, China, in 2012. She is currently pursuing the M.S. degree from the State Key Laboratory of Information Engineering in Surveying, Mapping, and Remote Sensing (LIESMARS), Wuhan University, Wuhan, China.

Her research interests include image information extraction and multi/hyperspectral image classification.

Jón Atli Benediktsson (F'14) received the Cand. Sci. degree in electrical engineering from the University of Iceland, Reykjavik, and the M.S.E.E. and Ph.D. degrees in electrical engineering from Purdue University, West Lafayette, IN, USA, in 1984, 1987, and 1990, respectively.

He is currently a Pro Rector for Academic Affairs and a Professor of Electrical and Computer Engineering with the University of Iceland, Reykjavík, Iceland. His research interests include remote sensing, biomedical analysis of signals, pattern recognition, image processing, and signal processing, and he has published extensively in those fields.

Prof. Benediktsson was the 2011–2012 President of the IEEE Geoscience and Remote Sensing Society (GRSS) and has been on the GRSS AdCom since 2000. He was the Editor-in-Chief of the IEEE TRANSACTIONS ON GEOSCIENCE AND REMOTE SENSING (TGRS) from 2003 to 2008 and has served as an Associate Editor of TGRS, the IEEE GEOSCIENCE AND REMOTE SENSING LETTERS, and the IEEE Access since 1999, 2003, and 2013. He is on the Editorial Board of the PROCEEDINGS OF THE IEEE and on the International Editorial Board of the *International Journal of Image and Data Fusion* and was the Chairman of the Steering Committee of IEEE JOURNAL OF SELECTED TOPICS IN APPLIED EARTH OBSERVATIONS AND REMOTE SENSING from 2007 to 2010. He is a Cofounder of the biomedical startup company Oxymap (www.oxymap.com). He is a Fellow of SPIE. He is a member of the Association of Chartered Engineers in Iceland (VFI), Societas Scinetiarum Islandica, and Tau Beta Pi. He received the Stevan J. Kristof Award from Purdue University in 1991 as an outstanding Graduate Student in remote sensing. In 1997, he was the recipient of the Icelandic Research Council's Outstanding Young Researcher Award, in 2000, he was granted the IEEE Third Millennium Medal, in 2004, he was a corecipient of the University of Iceland's Technology Innovation Award, in 2006, he received the yearly Research Award from the Engineering Research Institute of the University of Iceland, and in 2007, he received the Outstanding Service Award from the IEEE Geoscience and Remote Sensing Society. He was a corecipient of the 2012 IEEE Transactions on Geoscience and Remote Sensing Paper Award, and in 2013, he was a corecipient of the IEEE GRSS Highest Impact Paper Award. In 2013, he received the IEEE/VFI Electrical Engineer of the Year Award.

Liangpei Zhang (M'06–SM'08) received the B.S. degree in physics from Hunan Normal University, Changsha, China, the M.S. degree in optics from the Chinese Academy of Sciences, Xian, China, and the Ph.D. degree in photogrammetry and remote sensing from Wuhan University, Wuhan, China, in 1982, 1988, and 1998, respectively.

He is currently the Head of the Remote Sensing Division, State Key Laboratory of Information Engineering in Surveying, Mapping, and Remote Sensing, Wuhan University. He is also a Chang-Jiang Scholar Chair Professor appointed by the Ministry of Education of China, Beijing, China. He is currently a Principal Scientist for the China State Key Basic Research Project (2011–2016) appointed by the Ministry of National Science and Technology of China, Beijing, China, to lead the remote sensing program in China. He has more than 300 research papers. He is the holder of five patents. His research interests include hyperspectral remote sensing, high-resolution remote sensing, image processing, and artificial intelligence.

Dr. Zhang is a Fellow of the Institution of Engineering and Technology, an Executive Member (Board of Governor) of the China National Committee of the International Geosphere-Biosphere Programme, and an Executive Member of the China Society of Image and Graphics. He regularly serves as a Cochair of the series SPIE Conferences on Multispectral Image Processing and Pattern Recognition, Conference on Asia Remote Sensing, and many other conferences. He edits several conference proceedings, issues, and Geoinformatics symposiums. He also serves as an Associate Editor of the *International Journal of Ambient Computing and Intelligence*, the *International Journal of Image and Graphics*, the *International Journal of Digital Multimedia Broadcasting*, the *Journal of Geo-Spatial Information Science*, the *Journal of Remote Sensing*, and the IEEE TRANSACTIONS ON GEOSCIENCE AND REMOTE SENSING.

Jun Li (M'13) received the B.S. degree in geographic information systems from Hunan Normal University, Changsha, China, the M.E. degree in remote sensing from Peking University, Beijing, China, and the Ph.D. degree in electrical engineering from the Instituto de Telecomunicações, Instituto Superior Técnico (IST), Universidade Técnica de Lisboa, Lisbon, Portugal, in 2004, 2007, and 2011, respectively.

From 2007 to 2011, she was a Marie Curie Research Fellow with the Departamento de Engenharia Electrotécnica e de Computadores and the Instituto de Telecomunicações, IST, Universidade Técnica de Lisboa, Lisbon, Portugal, in the framework of the European Doctorate for Signal Processing (SIGNAL). She has also been actively involved in the Hyperspectral Imaging Network, a Marie Curie Research Training Network involving 15 partners in 12 countries and intended to foster research, training, and cooperation on hyperspectral imaging at the European level. Since 2011, she has been a Postdoctoral Researcher with the Hyperspectral Computing Laboratory, Department of Technology of Computers and Communications, Escuela Politécnica, University of Extremadura, Cáceres, Spain. Her research interests include hyperspectral image classification and segmentation, spectral unmixing, signal processing, and remote sensing.

Dr. Li has been a Reviewer of several journals, including the IEEE TRANSACTIONS ON GEOSCIENCE AND REMOTE SENSING, the IEEE GEOSCIENCE AND REMOTE SENSING LETTERS, *Pattern Recognition, Optical Engineering, Journal of Applied Remote Sensing, and Inverse Problems and Imaging*. She received the 2012 Best Reviewer Award of the IEEE JOURNAL OF SELECTED TOPICS IN APPLIED EARTH OBSERVATIONS AND REMOTE SENSING.

Antonio Plaza (M'05–SM'07) received the Computer Engineer degree in 1997, the M.Sc. degree in 1999, and the Ph.D. degree in 2002, all in computer engineering, from the University of Extremadura, Caceres, Spain.

He is an Associate Professor (with accreditation for Full Professor) with the Department of Technology of Computers and Communications, University of Extremadura, Badajoz, Spain, where he is the Head of the Hyperspectral Computing Laboratory (HyperComp). He was the Coordinator of the Hyperspectral Imaging Network, a European project with a total funding of 2.8 MEuro. He has authored more than 400 publications, including 119 JCR journal papers (71 in IEEE journals), 20 book chapters, and over 240 peer-reviewed conference proceeding papers (94 in IEEE conferences). He has guest-edited seven special issues on *JCR journals* (three in IEEE journals).

Prof. Plaza has been a Chair for the IEEE Workshop on Hyperspectral Image and Signal Processing: Evolution in Remote Sensing (2011). He is a recipient of the recognition of Best Reviewers of the IEEE GEOSCIENCE AND REMOTE SENSING LETTERS (in 2009) and a recipient of the recognition of Best Reviewers of the IEEE TRANSACTIONS ON GEOSCIENCE AND REMOTE SENSING (in 2010), a journal for which he has served as Associate Editor in 2007–2012. He is also an Associate Editor for IEEE Access and was a member of the Editorial Board of the IEEE GEOSCIENCE AND REMOTE SENSING NEWSLETTER (2011–2012) and the IEEE GEOSCIENCE AND REMOTE SENSING MAGAZINE (2013). He was also a member of the steering committee of the IEEE JOURNAL OF SELECTED TOPICS IN APPLIED EARTH OBSERVATIONS AND REMOTE SENSING (2012). He served as the Director of Education Activities for the IEEE Geoscience and Remote Sensing Society (GRSS) in 2011–2012 and is currently serving as President of the Spanish Chapter of IEEE GRSS (since November 2012). He is currently serving as the Editor-in-Chief of the IEEE TRANSACTIONS ON GEOSCIENCE AND REMOTE SENSING JOURNAL (since January 2013).

Mauro Dalla Mura (S'08–M'11) received the Laurea (B.E.) and Laurea Specialistica (M.E.) degrees in telecommunication engineering from the University of Trento, Trento, Italy, in 2005 and 2007, respectively. He received a joint Ph.D. degree in information and communication technologies (Telecommunications Area) from the University of Trento, Italy and in electrical and computer engineering from the University of Iceland, Reykjavik, Iceland, in 2011. In the same year, he was a Research Fellow with the Fondazione Bruno Kessler, Trento, Italy, conducting research on computer vision.

He is currently an Assistant Professor with the Grenoble Institute of Technology (Grenoble INP), Grenoble, France. He is conducting research at the Grenoble Images Speech Signals and Automatics Laboratory (GIPSA-Lab), Cedex, France. His research interests include remote sensing, image processing, and pattern recognition, in particular, mathematical morphology, classification, and multivariate data analysis.

Dr. Dalla Mura is a Reviewer of the IEEE TRANSACTIONS ON GEOSCIENCE AND REMOTE SENSING, the IEEE GEOSCIENCE AND REMOTE SENSING LETTERS, the IEEE JOURNAL OF SELECTED TOPICS IN EARTH OBSERVATIONS AND REMOTE SENSING, the IEEE JOURNAL OF SELECTED TOPICS IN SIGNAL PROCESSING, *Pattern Recognition Letters*, *ISPRS Journal of Photogrammetry and Remote Sensing, Photogrammetric Engineering, and Remote Sensing (PE&RS)*. He is a member of the Geoscience and Remote Sensing Society (GRSS) and the IEEE GRSS Data Fusion Technical Committee (DFTC) and Secretary of the IEEE GRSS French Chapter (2013–2016). He was a Lecturer at the RSSS12—Remote Sensing Summer School 2012 (organized by the IEEE GRSS), Munich, Germany. He was the recipient of the IEEE GRSS Second Prize in the Student Paper Competition of the 2011 IEEE International Geoscience and Remote Sensing Symposium 2011 (Vancouver, CA, July 2011).